Electronic Supplementary Information (ESI)

Metal-ion-dependent polarity switching and dielectric enhancement in solvent-vapour-responsive mononuclear complexes

Fumiya Kobayashi*[,a], Hiroki Iwase[a], Shoma Hoshino[b] and Makoto Tadokoro*[,a]

[a] Department of Chemistry, Faculty of Science, Tokyo University of Science, 1-3 Kagurazaka, Shinjuku-ku, Tokyo 162-8601, Japan.

[b] Department of Chemistry, School of Science, Kitasato University, 1-15-1 Kitazato, Minami-ku, Sagamihara-shi Kanagawa 252-0373, Japan.

Corresponding author:

F. Kobayashi, fkobayashi@rs.tus.ac.jp

M. Tadokoro, tadokoro@rs.tus.ac.jp

Table S1. Crystallographic data for **1**–**4**.

Compound	**1**	**2**	**3**	**4**
Temperature / K	173	90	90	90
Formula	$C_{18}H_{19}N_2FeO_5$	$C_{18}H_{19}N_2MnO_5$	$C_{19}H_{21}N_2FeO_5S$	$C_{19}H_{21}N_2MnO_5S$
Crystal system	Monoclinic	Monoclinic	Monoclinic	Triclinic
Space group	$P2_1/c$ (#14)	$P2_1/c$ (#14)	Cc (#9)	$P\bar{1}$ (#2)
a / Å	12.4010(10)	12.5148(5)	15.3544(5)	8.8350(3)
b / Å	16.4977(13)	16.7477(7)	17.1176(5)	10.5064(3)
c / Å	8.6621(7)	8.7014(3)	7.9303(2)	10.7201(4)
α / °	90	90	90	90.9370(10)
β / °	101.098(3)	102.542(2)	106.9600(10)	102.4160(10)
γ / °	90	90	90	91.6090(10)
V / Å^3	1739.0(2)	1780.24(12)	1993.67(10)	971.17(6)
Z	4	4	4	2
D_{calc} / g cm^{-3}	1.525	1.486	1.484	1.520
μ / mm^{-1}	0.899	0.773	0.894	0.821
F(000)	828	824	924	460
R_1, wR_2 ($I > 2\sigma(I)$)	0.0433, 0.1138	0.0363, 0.0902	0.0289, 0.0723	0.0321, 0.0752
R_1, wR_2 (for all data)	0.0493, 0.1190	0.0413, 0.940	0.0293, 0.0726	0.0337, 0.0761
GOF	1.058	1.065	1.026	1.073
Reflections/Parameters	3000/241	3137/385	3283/402	3198/402
Flack	-	-	0.068(11)	-
CCDC	2512678	2512679	2512680	2512681

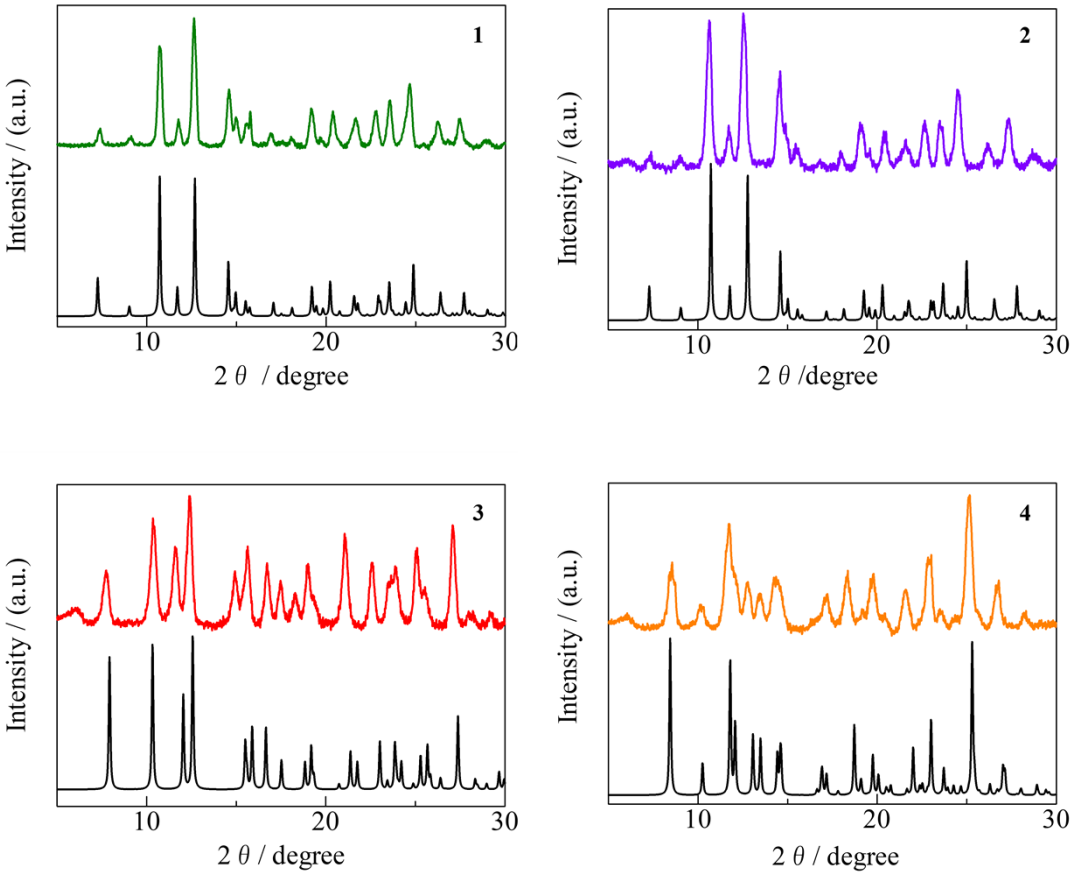

Figure S1. PXRD patterns for the crystalline sample of **1**–**4** at 298 K and their simulations (black).

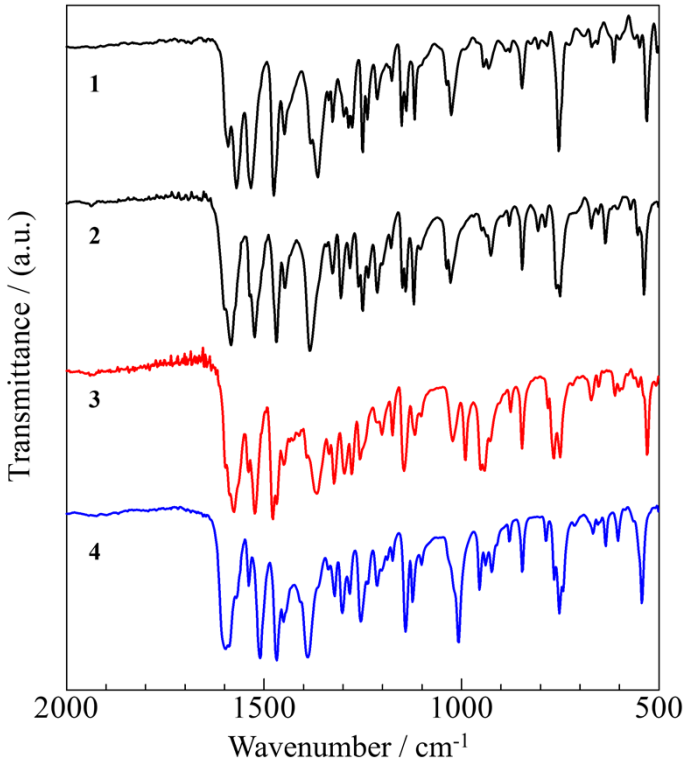

Figure S2. FT-IR spectra for **1**–**4**. Peaks observed at 1020 cm^{-1} for **3** and **4** are attributed to the S=O vibrations of DMSO.

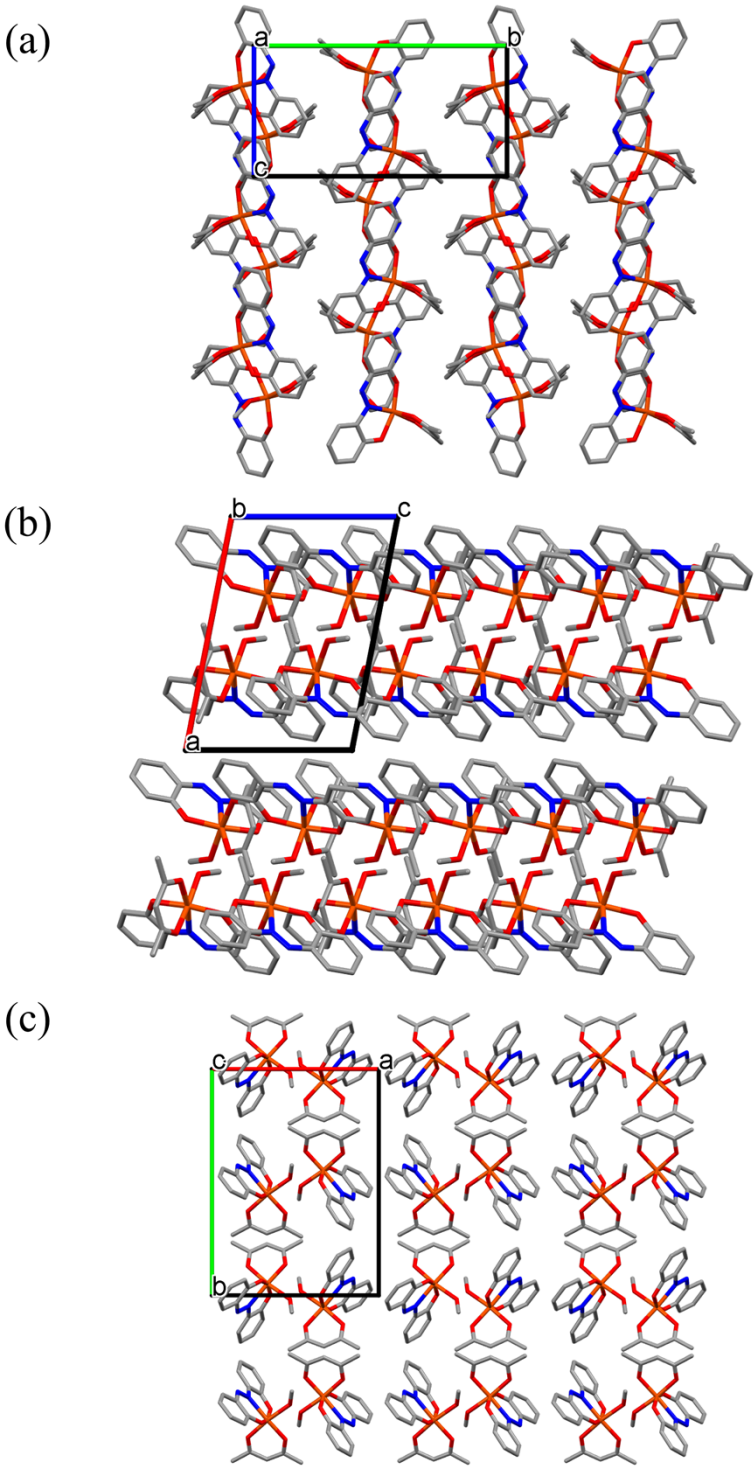

Figure S3. Crystal packing structures for **1** at 173 K along (a) *a*, (b) *b*, (c) *c* axes. Hydrogen atoms are omitted for clarity.

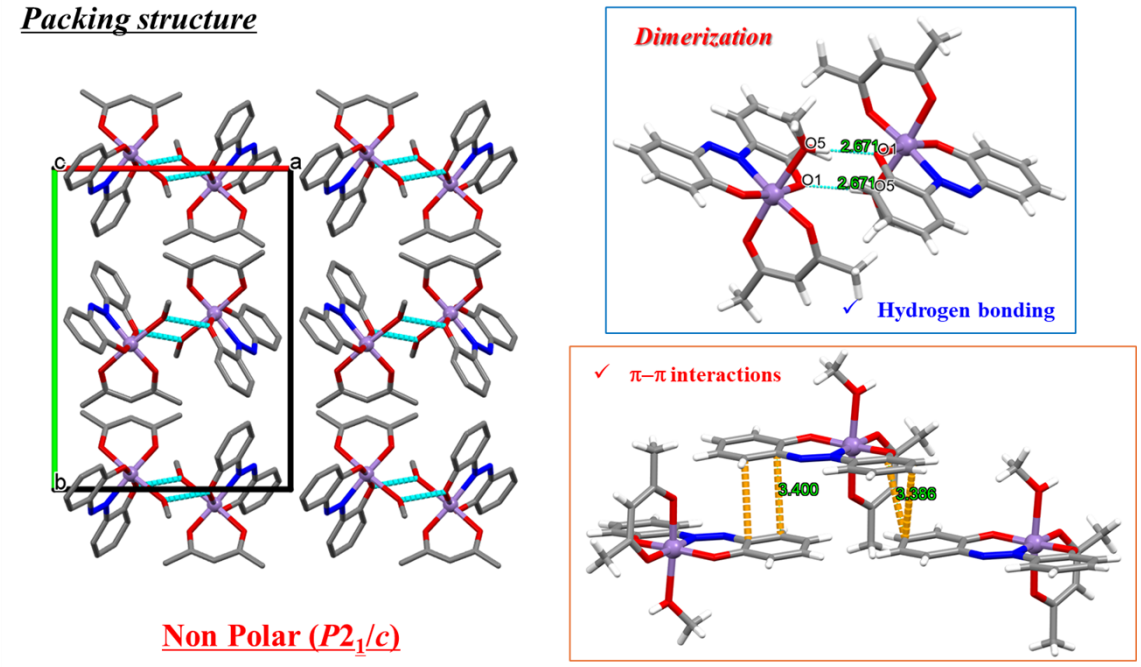

Figure S4. Crystal packing structure and intermolecular interactions of **2** at 90 K.

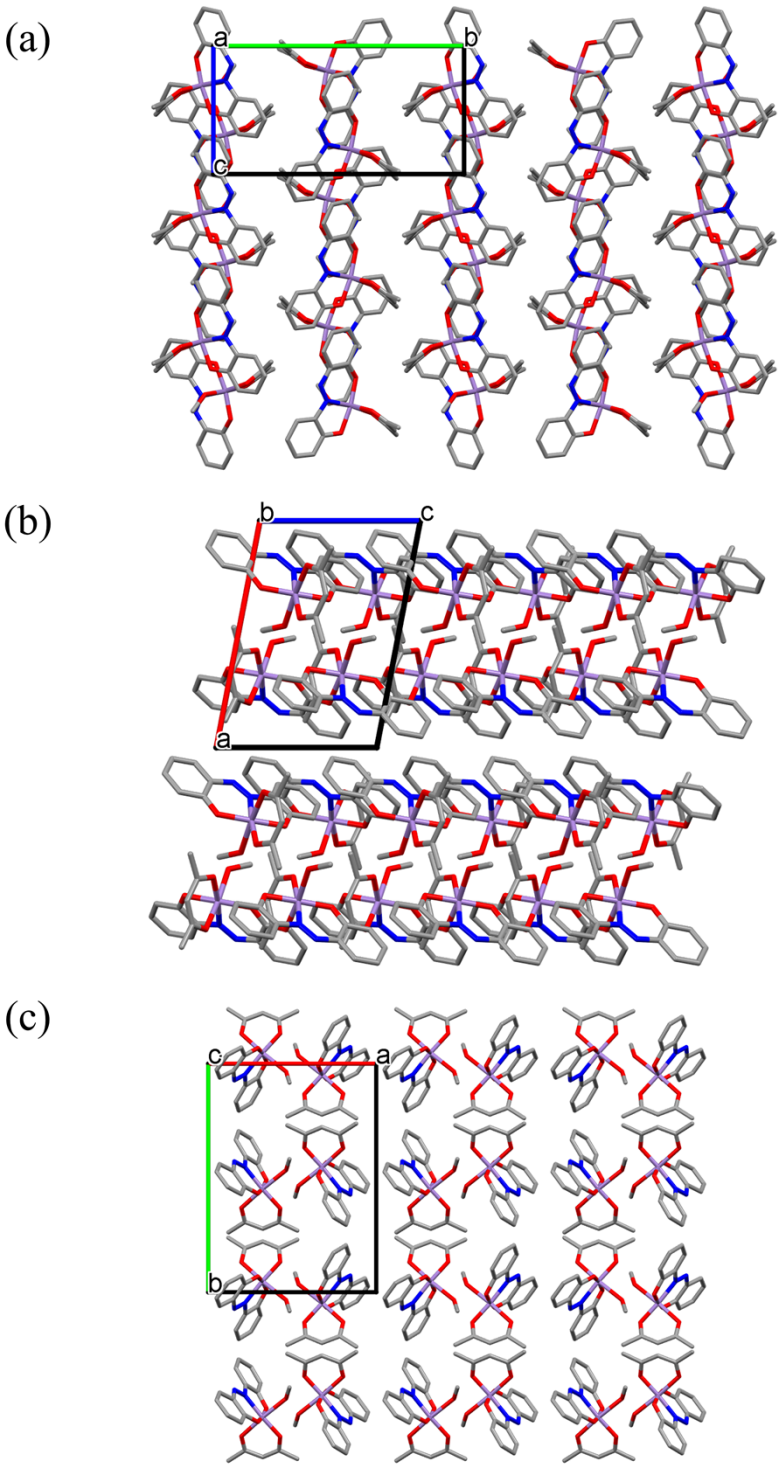

Figure S5. Crystal packing structures for **2** at 90 K along (a) *a*, (b) *b*, (c) *c* axes. Hydrogen atoms are omitted for clarity.

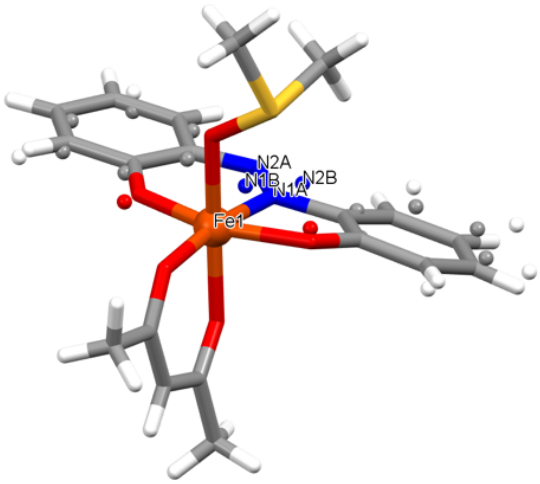

Figure S6. Crystal structure for **3** at 90 K with the atom-numbering scheme.

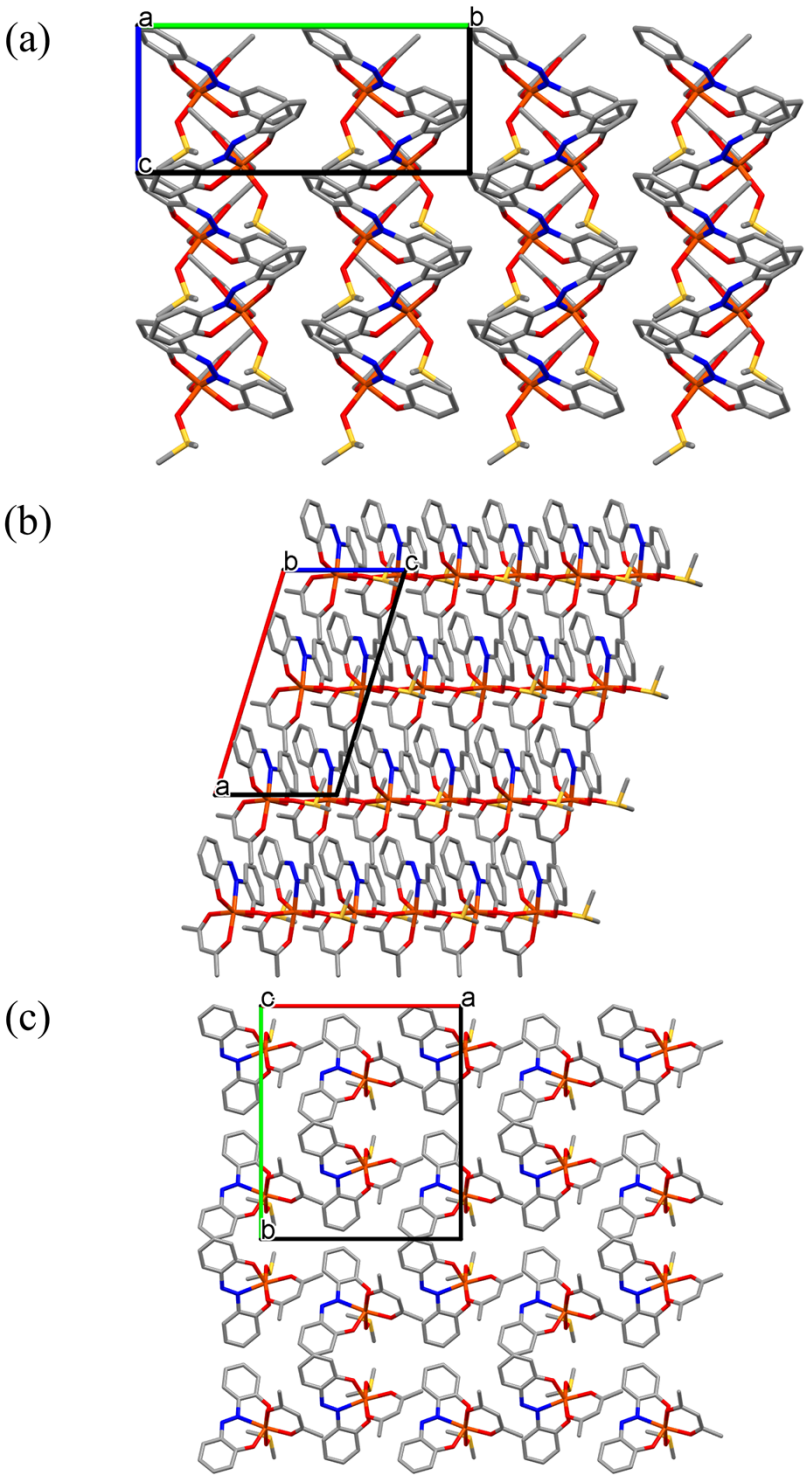

Figure S7. Crystal packing structures for **3** at 90 K along (a) *a*, (b) *b*, (c) *c* axes. Hydrogen atoms and disordered atoms are omitted for clarity.

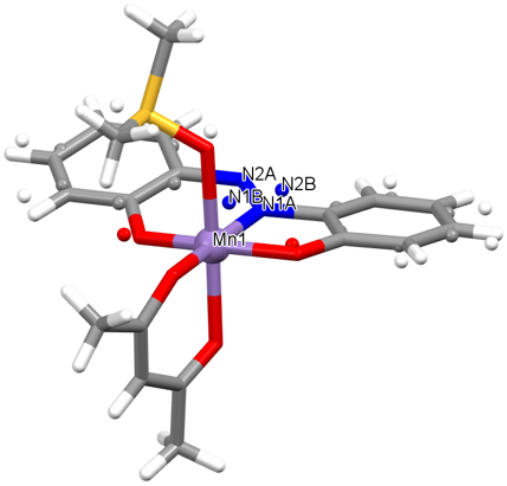

Figure S8. Crystal structure for **4** at 90 K with the atom-numbering scheme.

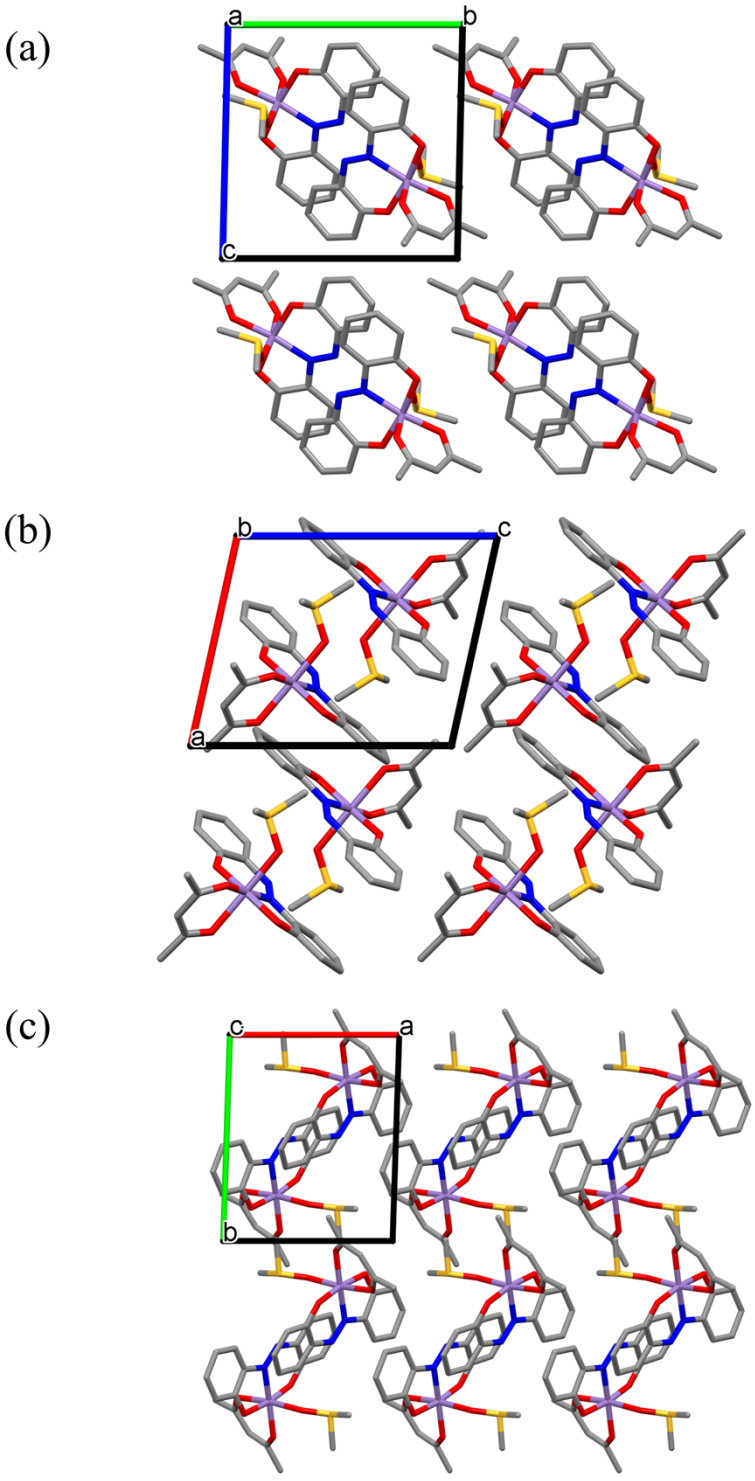

Figure S9. Crystal packing structures for **4** at 90 K along (a) *a*, (b) *b*, (c) *c* axes. Hydrogen atoms and disordered atoms are omitted for clarity.

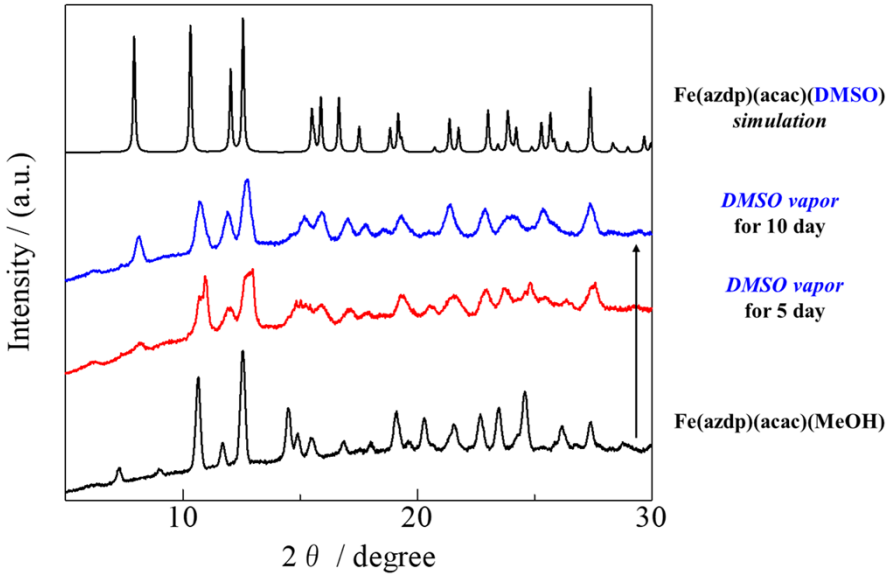

Figure S10. PXRD patterns for **1** and DMSO-vapor exposed samples (**1′**).

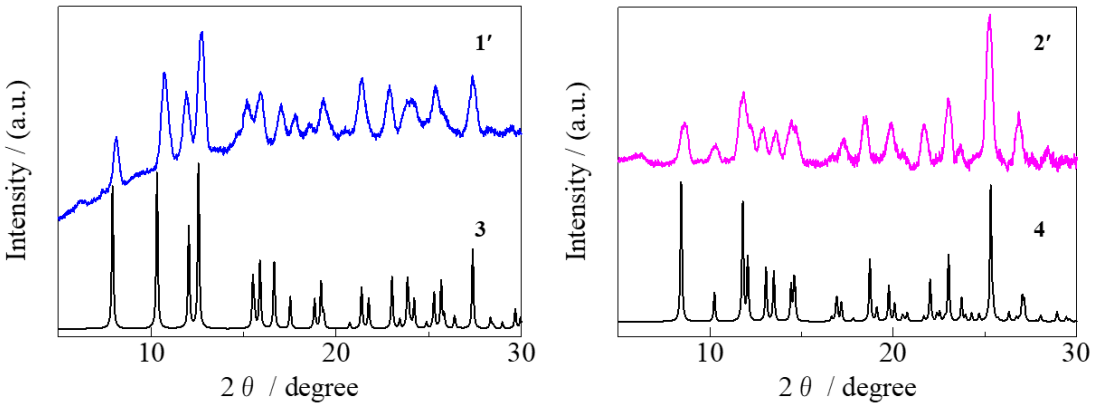

Figure S11. PXRD patterns for the crystalline samples of **1′** (blue) and **2′** (pink) at 298 K and the simulations for **3** and **4** (black).

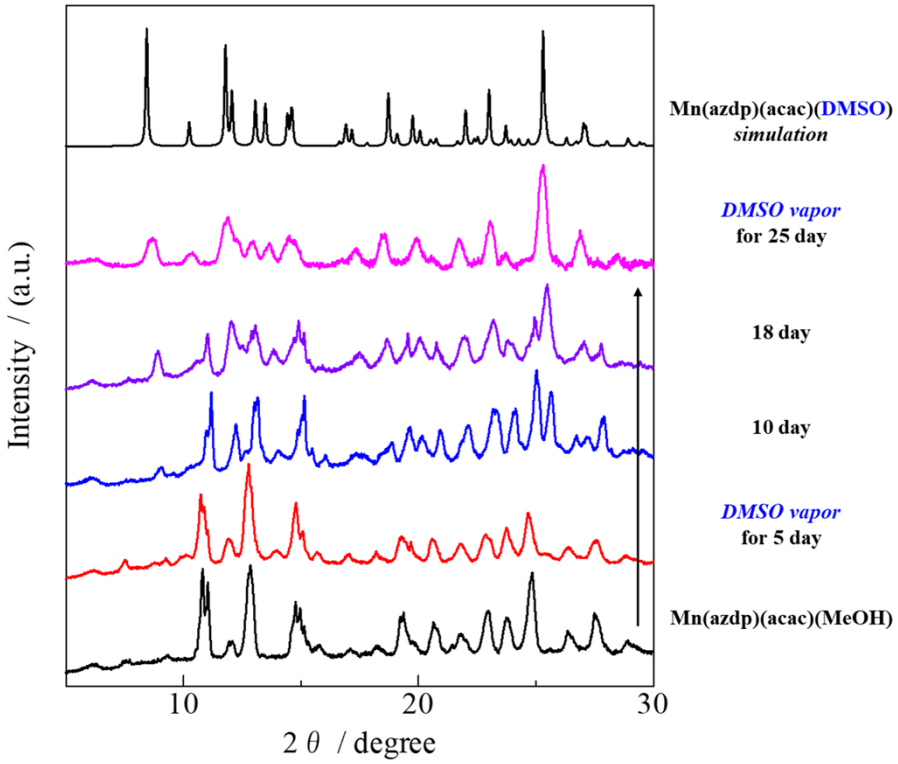

Figure S12. PXRD patterns for **2** and DMSO-vapor exposed samples (**2′**).

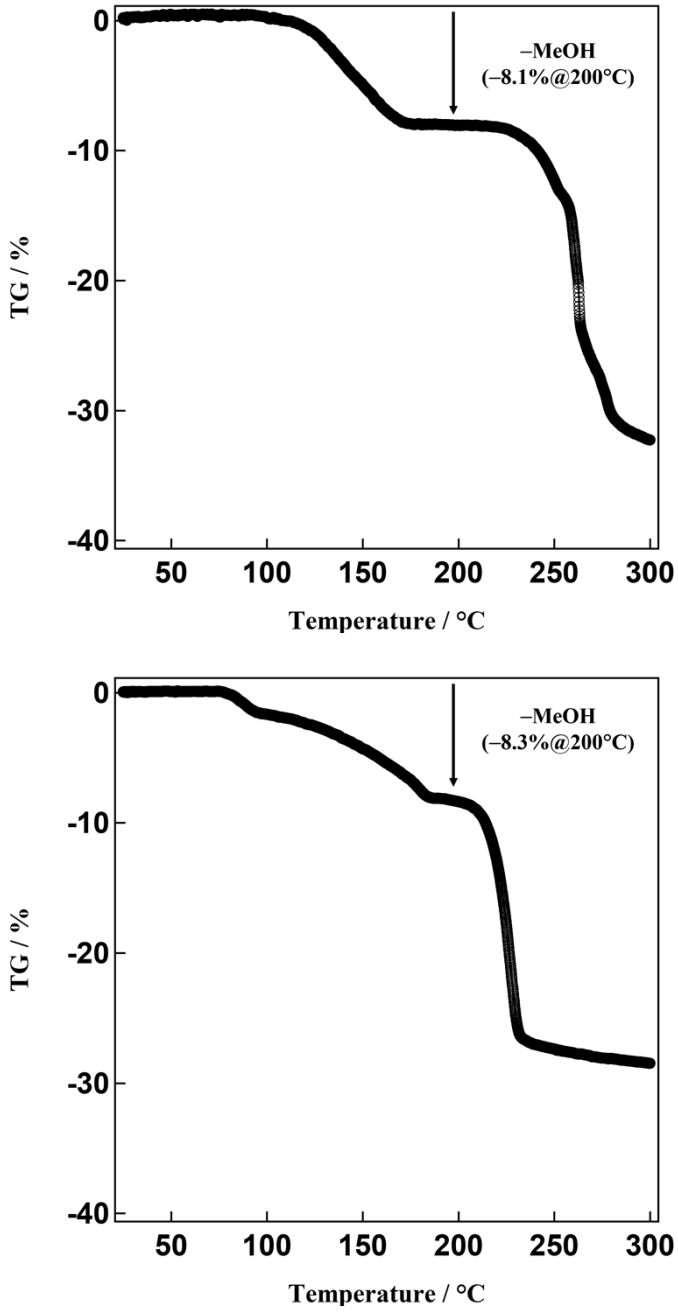

Figure S13. TGA curve for (top) **1** and (bottom) **2**. 8.1% and 8.3% weight losses were observed for **1** and **2** above 200 °C, respectively. This shows good agreement with the MeOH contents of **1** and **2** (MeOH = 8.0%). The weight loss over 250 °C corresponds to the decomposition of complexes.

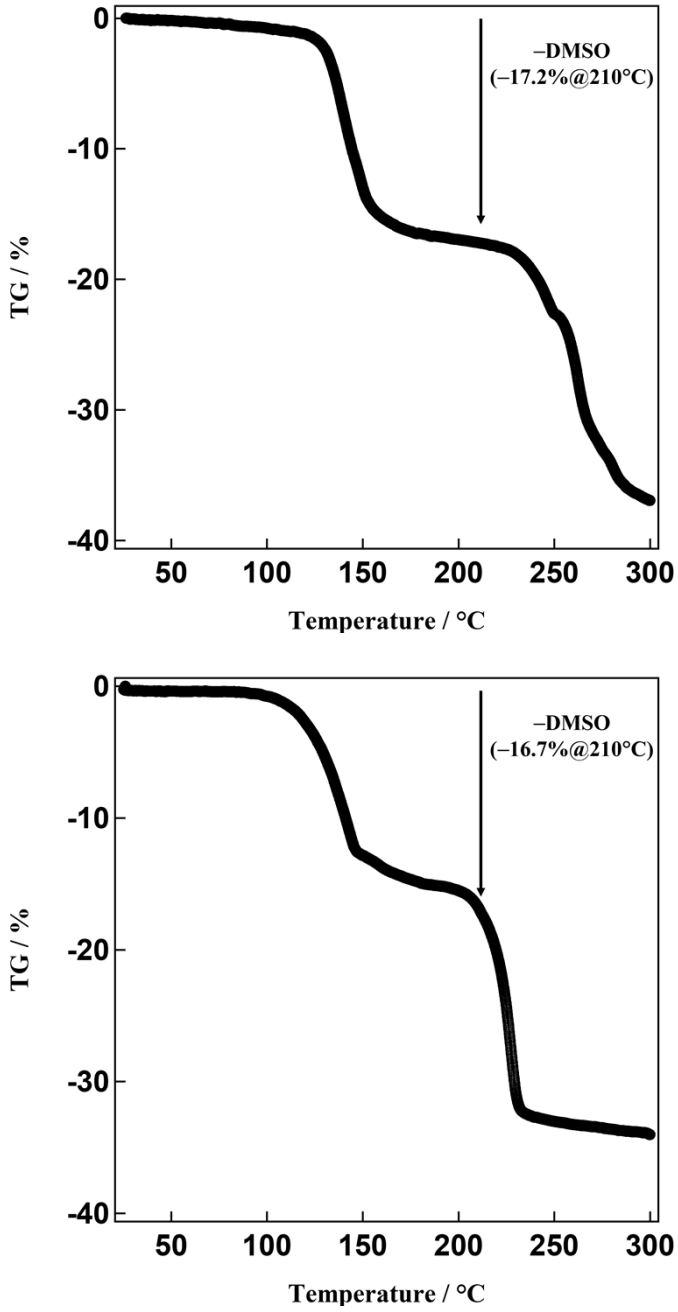

Figure S14. TGA curve for (top) **1′** and (bottom) **2′**. 17.2% and 16.7% weight loss were observed for **1′** and **2′** above 210 °C, respectively. This shows good agreement with the DMSO content of **1′** and **2′** (DMSO = 17.5%), respectively. The weight loss over 250 °C corresponds to the decomposition of complexes.